Communication

MRI Thermometry Based on PARACEST Agents

Shanrong Zhang, Craig R. Malloy, and A. Dean Sherry

J. Am. Chem. Soc., **2005**, 127 (50), 17572-17573• DOI: 10.1021/ja053799t • Publication Date (Web): 30 November 2005

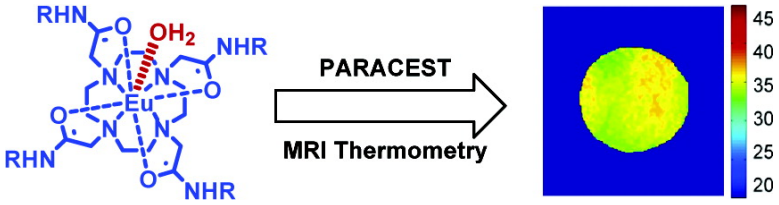

More About This Article

Additional resources and features associated with this article are available within the HTML version:

- Supporting Information
- Links to the 15 articles that cite this article, as of the time of this article download
- Access to high resolution figures
- Links to articles and content related to this article
- Copyright permission to reproduce figures and/or text from this article

View the Full Text HTML

J|A|C|S
COMMUNICATIONS

Published on Web 11/30/2005

MRI Thermometry Based on PARACEST Agents

Shanrong Zhang,*[,†,‡] Craig R. Malloy,[†] and A. Dean Sherry*[,†,§]

Advanced Imaging Resonance Center, University of Texas Southwestern Medical Center, 5323 Harry Hines Boulevard, Dallas, Texas 75390-8568, and Department of Chemistry, University of Texas at Dallas, P.O. Box 830688, Richardson, Texas 75083-0688

Received June 9, 2005; E-mail: zhangs@u.washington.edu; sherry@utdallas.edu

Noninvasive temperature monitoring has many medical applications because of the close inter-relationship between tissue temperature, metabolism, and physiology. Such applications include the monitoring of local hyperthermia for tumor ablation,[1] the treatment of heart arrhythmias,[2] the local drug delivery with thermosensitive microcarriers,[3,4] and the controlled release of gene therapy using heat-sensitive promoters.[5] Recently, magnetic resonance imaging (MRI) has been explored as a noninvasive technique for temperature mapping.[6] The temperature dependence of several physical parameters of water have been used for MRI thermometry, including diffusion (D),[7] spin lattice relaxation (T_1),[8] and shifts in the water proton resonance frequency (PRF).[9] Among these methods, PRF thermometry is most widely applied because it less dependent on tissue composition than the other parameters. This method is based on an early discovery of Hindman,[10] who found that the water proton resonance frequency decreases linearly by ca. 0.01 ppm/°C over the range of 37−43 °C. However, motion effects and magnetic field inhomogeneities can limit the error of this method to ±1−3 °C.[1] This level of accuracy is not problematic if the temperature differences are large (i.e., during tumor ablation) but is impractical if temperature differences are small. For example, the temperature heterogeneity in carotid atherosclerotic plaques is reportedly 0.2−0.3 °C.[11] Alternatively, exogenous probes based on either paramagnetic relaxation agents that alter T_1 or T_2[12,13] or hyperfine shift reagents that alter the chemical shift of some observable nucleus[14,15] are much more sensitive to temperature but suffer other experimental limitations for in vivo use largely related to the concentrations required and poor spatial resolution. Thus, a method that might allow accurate measures of small temperature differentials would be highly desirable. Here we report a novel MRI thermometric method based on the use of exogenous PARACEST[16] (*para*magnetic *c*hemical *e*xchange *s*aturation *t*ransfer) agents that sense and report temperature via the bulk water signal rather than a nucleus on the agent itself.

A new MRI contrast method was recently introduced, where the bulk water signal intensity is altered via chemical exchange saturation transfer (CEST).[17] This was later extended to paramagnetic systems, and such small molecule agents are now referred to as PARACEST agents.[16] By selective presaturation of highly shifted spin pool, A (i.e., $Ln^{3+}-H_2O$ or Ln^{3+}−amide protons), the MRI signal intensity of any exchanging spin partner, B (i.e., bulk water), will decrease in intensity if the kinetics are appropriate. For a simple two-site exchange system,[16] this may be described by $M_{SB}/M_{0B} \approx (1 + k_{BA}T_{1B})^{-1}$, where M_{SB} and M_{0B} are ^{1}H signal intensities of B (bulk water) with and without presaturation of spin A; T_{1B} is the spin lattice relaxation time of B, and k_{BA} is the exchange rate constant of water from B to A. Since k_{BA} is directly related to temperature via the classical Arrhenius equation, changes in M_{SB}/M_{0B} may be used to measure temperature if the agent concentration is known.[18] This requirement is difficult for in vivo applications because here the agent concentration is usually unknown. However, a second temperature-dependent feature of such systems is the hyperfine position (δ, in ppm) of the exchanging site on the PARACEST agent; for example, hyperfine shift of lanthanide-bound water protons ($Ln^{3+}-H_2O$) can vary from +500 ppm for typical Tm^{3+} complexes to −800 ppm for Dy^{3+} complexes.[19] Such hyperfine shifts are highly temperature dependent,[20] and this feature has been the basis of previous shift reagent-based thermometry experiments.[14,15] PARACEST thermometry, however, differs in that the MRI readout signal is from bulk water present at ca. 55 M, thereby offering the potential of thermometry measurements with high spatial resolution. Variable-temperature data (Figure S1) indicate that the ^{1}H chemical shift of the Ln^{3+}-bound water resonance vary linearly over 20−50 °C according to $\delta_{PPM} = 6.9 \times T - 944.7$ for Dy(**1**)$^{3+}$ and $\delta_{PPM} = -0.4 \times T + 64.6$ for Eu(**2**)$^-$ (Scheme 1). These temperature responses are ∼690- and ∼40-fold greater than the PRF response (−0.01 ppm/°C).

The key to PARACEST thermometry then is to locate the ^{1}H chemical shift (δ) of the Ln^{3+}-bound water molecule in images with high spatial resolution. This may be accomplished by measuring the residual bulk water Z magnetization after a series of selective presaturation pulses that are varied over a small range of frequencies spanning the Larmor frequency of the Ln^{3+}-bound water molecule.[21] For temperature imaging, this may be expanded to three-dimensional space by acquiring one image at each saturation offset (Scheme 2). By tracing the intensity changes of a specific imaging pixel along the imaging series (Figure S2), a plot of pixel intensity versus frequency offset yields a typical Z spectrum. The temperature of this pixel is obtained by identifying the minimum intensity point

Scheme 1. Molecular Structures of Ligands **1** and **2**

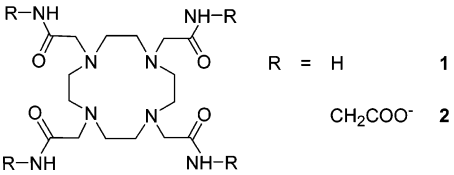

Scheme 2. Basic Procedure for Generating a Temperature Map Based on PARACEST MRI Thermometry

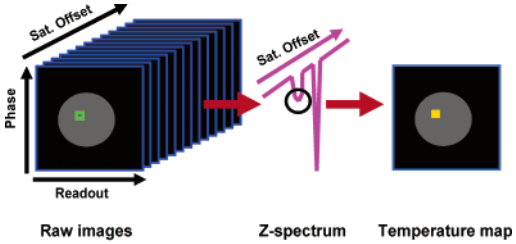

† University of Texas Southwestern Medical Center.
‡ Current address: Department of Radiology, University of Washington, Box 357115, 1959 NE Pacific St., Seattle, Washington 98195-7115.
§ University of Texas at Dallas.

10.1021/ja053799t CCC: $30.25

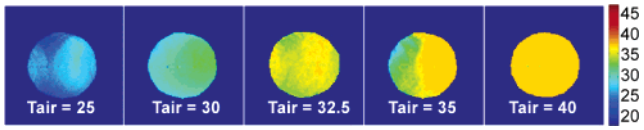

Figure 1. Temperature maps of a phantom containing 1 mL of 10 mM Eu(**2**)$^-$ in water at pH 7.0. The temperatures of the air flowing over the sample are indicated in each figure, while those reported by imaging are shown by the color bar (in units of °C).

which corresponds to the chemical shift of the Ln^{3+}-bound water. Substitution into one of the linear relationships reported above yields the temperature in that pixel. A similar procedure is then repeated for all pixels in the image or region of interest to generate a temperature map.

To test the feasibility of this method, a 1 cm o.d. vial containing 10 mM Eu(**2**)$^-$ in water (pH 7) was imaged at different controlled temperatures using a 2 cm RF surface coil and a 4.7 T animal imaging magnet. Typically, a series of CEST images were obtained by applying a 2 s presaturation pulse (B_1 = 735 Hz) over a small range of frequencies surrounding the Eu^{3+}-bound water position (50 ppm). In each case, a minimum was observed in M_{SB}/M_{0B} over this frequency range, and the frequency of this minimum provided a direct readout of temperature using the appropriate linear equation. The temperature images illustrated in Figure 1 show that even small temperature gradients across this 1 cm vial are easily detected by MRI. The temperature images as indicated by the color bars matched closely to those of the regulated air flowing over the sample. An in-plane temperature spatial resolution of 0.15 × 0.15 mm^2 was obtained using this phantom. The temporal resolution (~3 min) of the experiment could be improved substantially by varying the saturation frequency over a narrower frequency range that spans the expected bound water resonance frequency and by using shorter presaturation periods.[16]

Although this method offers considerable potential for in vivo temperature mapping, factors such as RF power deposition (SAR limits), inherent tissue magnetization transfer (MT) effects, the tissue biodistribution and toxicity of such complexes, and the exchange properties of a PARACEST agent in tissue must be assessed. It is important to point out that values of k_{BA} and T_{1B} need not be known a priori for temperature mapping; the only requirement is that these physical parameters be appropriate for CEST. T_{1B} is, of course, a feature of tissue water and cannot be easily changed, while k_{BA} is controlled by both the lanthanide ion and the ligand structure.[19] Clearly, optimal PARACEST agents for temperature mapping can be identified by adjusting these chemical variables. Imaging studies have been performed in animals after infusion of negatively charged LnDOTA−tetraamide complexes similar to Eu(**2**)$^-$ without adverse side effects,[22] so we anticipate that Eu(**2**)$^-$ will be well tolerated in vivo at the concentrations required for PARACEST thermometry. The RF power requirements depend on many factors, including coil design, volume of power deposition, and features of the PARACEST agent itself,[16] but others have shown that in vivo CEST imaging can be performed within acceptable SAR limits.[23] Finally, the inherent tissue MT effect could potentially interfere with PARACEST temperature mapping depending on the magnitude of the MT effect in the tissue under investigation. If needed, corrections for MT could be performed by measuring asymmetry differences between presaturation frequencies on each side of the bulk water resonance.[23]

In summary, the feasibility of PARACEST-based MRI thermometry has been demonstrated in vitro. In comparison with the classical PRF thermometry, the temperature responses of this method are substantially improved by factors of ~690- and ~40-fold for two prototype systems, Dy(**1**)$^{3+}$ and Eu(**2**)$^-$. This method is especially attractive because the imaging readout signal is bulk water (55 M), which offers the potential of much higher MRI spatial resolution than current spectral imaging methods.

Acknowledgment. This work was supported in part by grants from the Robert A. Welch Foundation (AT-584) and the National Institutes of Health (CA-115531 and RR-02584).

Supporting Information Available: The Experimental Section, two plots of bound water chemical shifts versus temperature for Dy(**1**)$^{3+}$ and Eu(**2**)$^-$ (Figure S1), a representative series of raw images for a phantom containing 1 mL of 10 mM Eu(**2**)$^-$ at 25 °C (Figure S2), and an experimental Z spectrum of a typical pixel along the saturation frequency offsets (Figure S3). This material is available free of charge via the Internet at http://pubs.acs.org.

References

(1) Weidensteiner, C.; Quesson, B.; Caire-Gana, B.; Kerioui, N.; Rullier, A.; Trillaud, H.; Moonen Chrit, T. W. *Magn. Reson. Med.* **2003**, *50*, 322.
(2) Levy, S. *Arch. Mal. Coeur Vaiss* **1995**, *88*, 1465.
(3) Weinstein, J. N.; Magin, R. L.; Yatvin, M. B.; Zaharko, D. S. *Science* **1979**, *204*, 188.
(4) Kim, S. *DRUGS IN R&D* **1993**, *46*, 618.
(5) Madio, D.; van Gelderen, P.; Olson, A.; de Zwart, J.; Fawcett, T.; Holbrook, N.; Mandel, M.; Moonen, C. *J. Magn. Reson. Imaging* **1998**, *8*, 101.
(6) Quesson, B.; Zwart, J. A. d.; Moonen, C. T. W. *J. Magn. Reson. Imaging* **2000**, *12*, 525.
(7) Le Bihan, D.; Delannoy, J.; Levin, R. L. *Radiology* **1989**, *171*, 853.
(8) Parker, D. L.; Smith, V.; Sheldon, P.; Crooks, L. E.; Fussell, L. *Med. Phys.* **1983**, *10*, 321.
(9) Ishihara, Y.; Calderon, A.; Watanabe, H.; Mori, K.; Okamoto, K.; Suzuki, Y.; Sato, K.; Kuroda, K.; Nakagawa, N.; Tsutsumi, S. In *Eleventh Annual Meeting of the Society of Magnetic Resonance in Medicine*; Berkeley, CA, 1992; p 4803.
(10) Hindman, J. C. *J. Chem. Phys.* **1966**, *44*, 4583.
(11) Casscells, W.; Hathorn, B.; David, M.; Krabach, T.; Vaughn, W. K.; McAllister, H. A.; Bearman, G.; Willerson, J. T. *Lancet* **1996**, *347*, 1447.
(12) Fossheim, S. L.; ll'yasov, K. A.; Wiggen, U. N.; Rogstad, A.; Hennig, J.; Klaveness, J.; Bjornerud, A. In *ISMRM*; Philadelphia, PA, 1999; p 725.
(13) Muller, R. N.; Vander Elst, L.; Laurent, S. *J. Am. Chem. Soc.* **2003**, *125*, 8405.
(14) Zuo, C. S.; Bowers, J. L.; Sherry, A. D.; Clouse, M. E. *Radiology* **1995**, *197*, 423.
(15) Hekmatyar, S. K.; Hopewell, P.; Pakin, S. K.; Babsky, A.; Bansal, N. *Magn. Reson. Med.* **2005**, *53*, 294.
(16) Zhang, S.; Merritt, M.; Woessner, D. E.; Lenkinski, R. E.; Sherry, A. D. *Acc. Chem. Res.* **2003**, *36*, 783.
(17) Ward, K. M.; Aletras, A. H.; Balaban, R. S. *J. Magn. Reson. Imaging* **2000**, *143*, 79.
(18) Terreno, E.; Castelli, D. D.; Cravotto, G.; Milone, L.; Aime, S. *Invest. Radiol.* **2004**, *39*, 235.
(19) Zhang, S.; Sherry, A. D. *J. Solid State Chem.* **2003**, *171*, 38.
(20) Peters, J. A.; Huskens, J.; Raber, D. J. *Prog. Nucl. Magn. Reson. Spectrosc.* **1996**, *28*, 283.
(21) Grad, J.; Bryant, R. G. *J. Magn. Reson. Imaging* **1990**, *90*, 1.
(22) Raghunand, N.; Howison, C.; Sherry, A. D.; Zhang, S. R.; Gillies, R. J. *Magn. Reson. Med.* **2003**, *49*, 249.
(23) Zhou, J. Y.; Lal, B.; Wilson, D. A.; Laterra, J.; van Zijl, P. C. M. *Magn. Reson. Med.* **2003**, *50*, 1120.

JA053799T